A Computational Study of the OH(OD) + CO Reactions: Effects of Pressure, Temperature, and Quantum-Mechanical Tunneling on Product Formation

R. S. Zhu, E. G. W. Diau,† M. C. Lin,* and A. M. Mebel‡

Department of Chemistry, Emory University, Atlanta, Georgia 30322

Received: February 7, 2001; In Final Form: October 1, 2001

The effects of pressure, temperature, and quantum-mechanical tunneling on the formation of CO_2 and H(D) atoms in the OH(OD) + CO reactions have been investigated by a multichannel RRKM calculation using the potential energy surface obtained by various high-level computational techniques including the G2 and modified G2 (G2M) methods. The strong non-Arrhenius behavior of the bimolecular rate constant for the OH + CO reaction was found to result from the combination of temperature, pressure, and quantum-mechanical tunneling. The effects of the latter two factors dominate at low temperatures, resulting in the significant leveling-off of the Arrhenius plot. The rapid increase in the rate constant above 1000 K was found to result from the sharp increase in the vibrational partition function of the transition state leading to CO_2 product formation. The observed strong isotope effect (k_H/k_D) can also be reasonably accounted for by the combined T, P and tunneling effects. The absolute values of the total rate constant were found to be controlled primarily by the barrier heights at TS1 and TS2 for the formation of HOCO and H + CO_2 products, respectively, and independent of the two weakly bound van der Waals precursor complexes, OHOC and OHCO. The barriers, which account best for the bulk of experimental data are 0.8 and 2.0 kcal/mol, respectively, within the ranges of our predicted values 1.0 and 2.3 kcal/mol based on different methods with about 1 (or ± 0.5) kcal/mol spread in the values.

1. Introduction

The reaction of the OH radical with CO is of great importance to hydrocarbon combustion[1,2] and atmospheric chemistry.[3] In combustion, the reaction is a major energy-releasing step, producing CO_2 and regenerating an H atom, which is a key chain-carrier in the combustion process. In tropospheric chemistry, the reaction is a major step involved in the HO_x cycle. Accordingly, numerous kinetic measurements have been carried out for the reaction, using a variety of techniques covering a wide range of experimental conditions.[4−45]

Figure 1 summarizes some of the modeled and directly determined kinetic data to illustrate the existing large scatter and the non-Arrhenius behavior, revealed by the large body of the experimental data. The strong non-Arrhenius temperature dependence has been qualitatively interpreted in terms of the conventional transition-state theory (CTST) assuming a single transition state.[9,31,46] Some interpretations took into consideration the involvement of the long-lived HOCO intermediate

$$\mathrm{OH + CO} \overset{\mathrm{TS1}}{\longleftrightarrow} \mathrm{HOCO} \overset{\mathrm{TS2}}{\longleftrightarrow} \mathrm{H + CO_2}$$

to account for the observed temperature and pressure effects.[20−22,47−50] The HOCO radical is known to exist in matrixes[51] and in the gas phase.[52−55]

The dynamics of the fragmentation of the HOCO formed in the H + CO_2 reaction has been studied extensively by Wittig, Zewail, and Simons among others.[56−62] Their elegant experiments firmly establish the mechanism given above, connecting the OH + CO reactants and the H + CO_2 products, or vice versa, with the HOCO intermediate.

Theoretically, the OH + CO reaction has been investigated by Schatz, Clary, and others[63−67] using different methods with varying degrees of approximation. Frost et al.[21] carried out a Rice−Ramsperger−Kassel−Marcus (RRKM) calculation to interpret their low temperature (80−297 K) experimental data by assuming a hydrogen-bonded complex (OH−CO) between OH and CO, and this complex may provide a precursor state for the formation of an energized HOCO radical via a transition state. The effects of tunneling, pressure, and temperature were taken into consideration in their study. However, the adjustment of the energies of TS1 and TS2 did not provide a good agreement between the experimental and calculated results at lower temperatures. More recently, Troe and co-workers,[39] and Golden et al.[50] modeled the experimental data phenomenologically in the temperature ranges of 80−2800 K and 253−2600 K, respectively, by adjusting some TS parameters to fit the experimental data. Most of the modeling was based on the potential energy surface (PES) of Schatz et al.[64 (a)] This and other ab initio PES results[68−73] show that the two possible complexes, HOCO and HCO_2, may be formed in the OH + CO reaction. In a study by Aoyagi and Kato,[73] the multiconfiguration self-consistent field (MCSCF) and configuration interaction (CI) methods were used to calculate the PES and the rate constant of the reaction. Their theoretical rate constant revealed a dramatic effect of quantum-mechanical tunneling which might account for the strong non-Arrhenius behavior.

To account for the combined effects of pressure, temperature, and quantum-mechanical tunneling, one must solve the coupled master equation for the chemical activation, collisional stabilization and decomposition processes; the latter process should also properly correct for the tunneling probability under the pressure-

* To whom correspondence should be addressed. E-mail: chemmcl@emory.edu.

† Current address: Department of Chemistry, The California Institute of Technology, Pasadena, California.

‡ Current address: Institute of Atomic and Molecular Sciences, Taipei, Taiwan.

10.1021/jp0104536 CCC: $20.00
Published on Web 11/16/2001

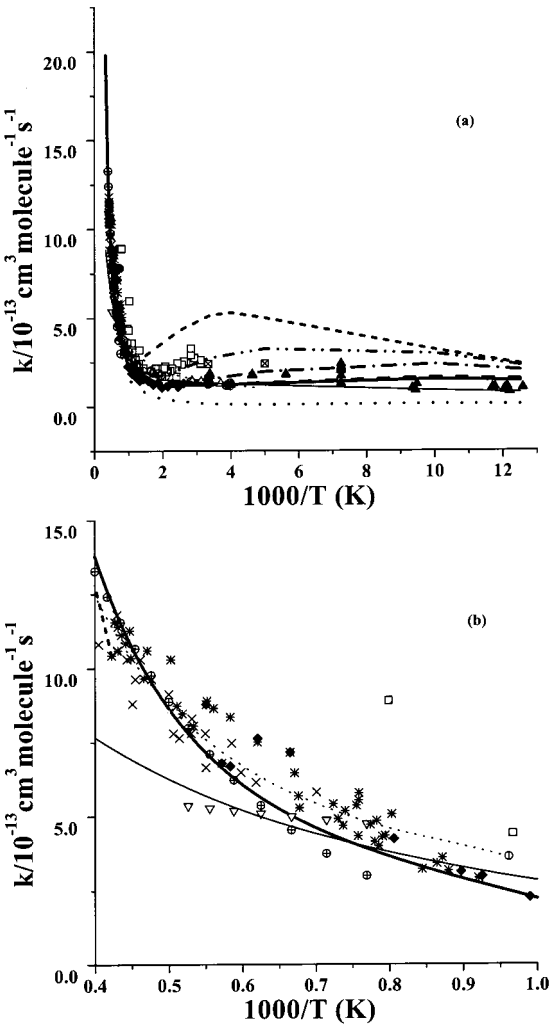

Figure 1. (a) Survey of the rate constant for the OH + CO reaction (M=Ar). The symbols are for the experimental results obtained by kinetic modeling, direct and indirect measurements. (b) An enlarged plot for clear illustration of high-temperature data. The symbols in (a) and (b) are as follows: □ (ref 17), ●(ref 40), ×(ref 50) ○ (ref 42), □ (ref 43), ▽ (ref 37), ⊕ (ref 38), △ (ref 14), ▲ (ref 21), ◆(ref 34), * (ref 35); the curves are the RRKM predictions from this study, dotted line (5 Torr without tunneling, this work), solid, dashed, dash−dotted, dosh-dot-dotted and short-dashed lines are the results of this work with tunneling at 5 Torr, 10 Torr, 100 Torr, 1 atm. and 10 atm, the curves are shown from bottom to top in the figure, respectively; the thinner solid line is the fitting result at 5 Torr in He (ref 39) and the thinner dotted line is the result from ref 50.

dependent (non-Boltzmann) condition.[74] In the present study, we apply the similar approach as that employed in our previously study of the H(D) + N_2O → H(D)N_2O→N_2OH(D) →N_2 +OH(D) process,[74] to examine the P, T, and tunneling effects on the OH(OD) + CO reactions. The effects of energy and angular-momentum (i.e., E, J-resolved) have been examined by means of the recently available Variflex code written by Klippenstein et al.[75] To more reliably evaluate these effects, we have also performed ab initio MO calculations for the PES of the OH (OD) + CO ⇌ H(D)OCO ⇌ H(D) + CO_2 systems using various methods including the Gaussian-2 method[76,77] and its modified version by Mebel et al. [78]

2. Computational Methods

2.1 Ab Initio Calculations. The geometries of the HOCO intermediates, the transition states, the reactants, and the products were optimized at the QCISD (quadratic configuration interaction with single and double substitutions) and B3LYP (i.e., Becke's three-parameter nonlocal exchange functional[79−81] with nonlocal correlation functional of Lee et al.[82] as well as the MP2 (second-order Møller−Plesset Perturbation) methods with different basis sets.[76,77,83,84] The energies of all species were also calculated by the G2Q[84] and G2M[78] schemes. The former implemented the Gaussian-2 method[77(b)] based on the optimized QCISD geometry. The G2M method uses a series of calculations with the B3LYP optimized geometry to approximate the CCSD-(T)/6-311+G(3df,2p) level of theory, including a "higher level correction" based on the number of paired and unpaired electron. The total G2M energy is calculated as follows[78]

$$E[(\mathrm{G2M(CC2)}] = E_{\mathrm{bas}} + \Delta E(+) + \Delta E(\mathrm{2df}) + \Delta E(\mathrm{CC}) + \Delta' + \Delta E\ (\mathrm{HLC, CC2}) + \mathrm{ZPE}$$

$$E_{\mathrm{bas}} = E[\mathrm{PMP4/6\text{-}311G(d, p)}]$$

$$\Delta E(+) = E[\mathrm{PMP4/6\text{-}311+G(d, p)}] - E_{\mathrm{bas}}$$

$$\Delta E(\mathrm{2df}) = E[\mathrm{PMP4/6\text{-}311G(2df,p)}] - E_{\mathrm{bas}}$$

$$\Delta E(\mathrm{CC}) = E[\mathrm{CCSD(T)/6\text{-}311G(d, p)}] - E_{\mathrm{bas}}$$

$$\Delta' = E[\mathrm{UMP2/6\text{-}311+G(3df,2p)}] - E[\mathrm{UMP2/6\text{-}311+G(2df,p)}] - E[\mathrm{UMP2/6\text{-}311+G(d,p)}] - E[\mathrm{UMP2/6-311(d,p)}]$$

$$\Delta E\ (\mathrm{HLC, CC2}) = -5.78n_{\beta} - 0.19n_{\alpha}\ \text{in units of mhartree}$$

All the calculations have been carried out using the GAUSSIAN98/DFT[76] and MOLPRO-96 programs.[85]

2.2 RRKM Calculations. Microcanonical RRKM calculations for the OH(OD) + CO reactions were performed by solving the master equation[74,75,86−92] involving multistep vibrational energy transfer for the excited intermediates ($HOCO^{\dagger}$ or $DOCO^{\dagger}$) with Wigner tunneling corrections[75] for the dissociation processes. The ab initio PES calculated at the G2M level to be discussed in the next section, was used to determine the reaction mechanism. The total thermal rate coefficient (k_{tot}) for the OH + CO reaction was computed by summing the individual thermal rate coefficients for both association and decomposition channels

$$k_{\mathrm{tot}} = k_{\mathrm{a}} + k_{\mathrm{b}} + k_{\mathrm{c}}$$

where k_{a} represents the association rate coefficient for the OH + CO via TS1 to form HOCO by collisional stabilization, k_{b} and k_{c} are the bimolecular rate constants for the formation of H + CO_2 via TS2 and TS3, respectively.

For our one-well system assumed in the present calculations, the master equation takes the form

$$\frac{\mathrm{d}\rho_i(t)}{\mathrm{d}t} = \phi_i + \omega\sum_{j=1}^{m} P_{ij}\,\rho_j(t) - \omega\rho_i(t) - (k_{i1} + k_{i2})\rho_i(t)$$

where ϕ_i represents the rate of OH + CO association reaction, m is the number of grains which is chosen such that the population of the mth grain contributes negligibly to the bimolecular rate coefficient, ω is the collision frequency (which is a function of temperature and pressure), $k_{i1}(E)$ and $k_{i2}(E)$ are the microcanonical rate coefficients for the decomposition and redissociation, and P_{ij} the probability of energy transfer from grain j to grain i upon collision. A simple exponential-down

model[75,86,92] was employed for P_{ij}

$$P_{ij} = A_j \exp[-\alpha(E_j - E_i)]; j \geq i$$

where α is a parameter governing the efficiency of energy transfer; α^{-1} corresponds to the average energy removed per collision for down collisions, $<\Delta E>_{down}$. A_j's are normalization constants satisfying the condition

$$\sum_i P_{ij} = 1$$

Much like our previous calculations with the Variflex code,[93] the component rates were evaluated at the *E*, *J*-resolved level.[75] The pressure dependence was treated by one-dimensional master equation calculations using the Boltzmann probability of the complex for the *J*-distribution. The master equation was solved by an inversion based approach[75,86] under the steady-state condition for the initial rate constants, $k_x(T,P)$ ($x = a,b,c$). The validity of the steady-state assumption will be addressed later. To achieve convergence in the integration over the energy range, an energy grain size of 10 cm^{-1} was used for 20−200 K and 80 cm^{-1} for 300−3000 K, these grain sizes provide numerically converged results for all temperatures studied with an energy spanning range, from 8000 cm^{-1} below to 55 920 cm^{-1} above the threshold. The total angular momentum *J* covered the range from 0 to 245 in steps of 5 for the *E*, *J*-resolved calculation. The effect of *J*-dependence was found to be negligible in the present system because the reaction has well-defined transition states. The numbers of states for all transition states were evaluated according to the rigid-rotor harmonic-oscillator assumption. The Variflex code[75] was employed in all rate constant calculations.

3. Results and Discussion

3.1 Geometries and Frequencies. *Geometries.* The optimized geometries of the products, intermediates, and transition states for the OH + CO reaction are shown in Figure 2. The hydroxyl radical reacts with the carbon monoxide molecule to form weakly bound linear van der Waals complexes OHOC and OHCO. The existence of OHCO, first pointed out by Kudla et al.,[64(c)] was confirmed experimentally by Lester et al.[94] and theoretically by Chakraborty and Lin.[95] In vdw-OHOC the forming H−O bond length is predicted to be 2.275 and 2.341 Å and the H−C bond length in vdw-OHCO predicted to be 2.345 and 2.419 Å, respectively, at B3LYP/6-311G (d,p) and MP2/6-311G(d,p) levels. Global scans of the HOCO intermolecular potential and IRC[96] calculations at B3LYP/6-311G(d,p) and MP2/6-311G(d,p) reveal that TS1 connects the collinear vdw-OHCO complex and trans-HOCO intermediate. The newly formed C−O bond length in trans-HOCO is about 0.6 Å shorter than that in TS1 and the C−O−H angle in trans-HOCO is enlarged by more than 10° from that of TS1 according to the geometries optimized at MP2/6−311(d,p) and QCISD/6−311-(d,p) levels. There are slightly larger differences for the C═O bond length and C−O−H bond angle between TS1 and trans-HOCO in the structure optimized at the B3LYP/6-311G(d, p) level. TS2 connects cis-HOCO and the products H + CO_2; TS2 is a tight transition state. The breaking OH bond lengths increase by 0.358, 0.281 and 0.365 Å and the O−C−O angles enlarge by 26.5, 26.6, and 26.5° in TS2 compared with those of in cis-HOCO optimized at the B3LYP/6−311G(d,p), MP2/6−311G-(d,p) and QCISD/6−311(d,p) levels, respectively. The trans-HOCO can transform to the intermediate HCO_2 via TS3 and further dissociate to the final products H+CO_2 via TS4. Cis-HOCO and trans-HOCO are connected by TS5. The present results indicate that there are no significant differences among MP2 (also reported by Carmichael[72]), B3LYP, and QCISD geometries for both *cis*-HOCO and *trans*-HOCO isomers. However, a slightly tighter transition state geometry was obtained at the MP2 level of theory. For example, the forming C−O bond in TS1 was calculated to be 1.93, 1.97, 2.01, and 2.58 Å at MP2, QCISD, CCSD(T), and B3LYP, respectively, with a much larger value by B3LYP. Furthermore, the breaking H−O distance in TS2 was calculated to be 1.26, 1.34, 1.33, and 1.36 Å by the same sequence of the methods.

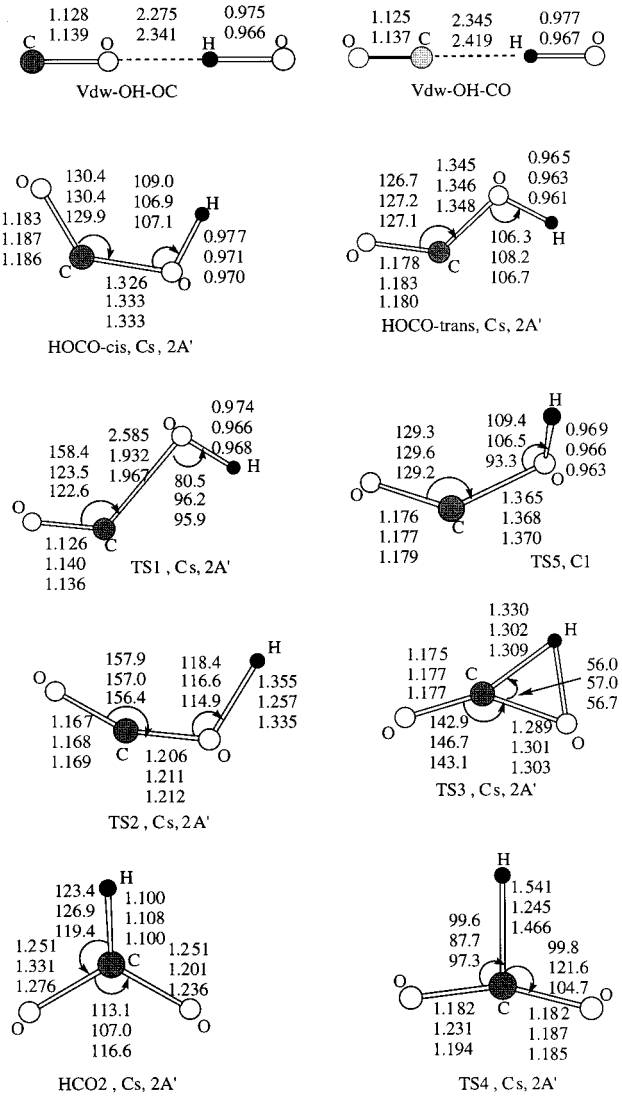

Figure 2. B3LYP/6-311G(d,p), MP2/6-311G(d, p), and QCISD/6-311G(d,p) optimized geometries of different species involved in the OH + CO reaction, values given from top to bottom, respectively.

Frequencies. Tables 1 and 2 list the frequencies and moments of inertia of the key species calculated at various levels for the reactions of OH + CO and OD + CO, respectively. One can see from these tables that vibrational frequencies obtained at different levels of theory have slight differences, but are in good agreement with experiment for both *cis*- and *trans*-HOCO (or DOCO).[97] However, the imaginary frequencies predicted for TS2 have large differences among the results obtained at QCISD/6-311G(d,p), CCSD(T)/6-311G(d,p), B3LYP/6-311G-(d,p), MP2/6-311G (d,p), and B3LYP/6-311G(d,p)//MP2/6-311G(d,p) levels; they are −2128.6, −2069.3, −1536.0, −3287.0, and −1626.2 cm^{-1}, respectively. When the tunneling effect is

TABLE 1: Vibrational Frequencies and Moments of Inertia of Some Key Intermediates and Transition States for the OH + CO Reaction Calculated at Various Levels[a]

species	I_a, I_b, I_c/au	ν_i/cm^{-1}
trans-HOCO[b]	10.9, 157.9, 168.8	528.2, 626.3, 1099.0, 1289.4, 1923.5, 3899.0
	(10.9, 157.2, 168.1)	(545.4, 622.3, 1083.6, 1243.0, 1909.2,3810.2)
	[10.9, 158.2, 169.1]	[532.4, 600.8, 1081.8, 1229.6, 1854.5, 3757.9]
	{10.9, 158.2, 169.1}	{513.4, 618.4, 1081.6, 1248.7, 1878.3, 3845.7}
cis-HOCO[b]	12.9, 153.2, 166.1	588.8, 615.1, 1106.5, 1344.5, 1883.1, 3738.1
	(12.7, 152.8, 165.6)	(602.6, 616.6, 1081.3, 1304.1, 1876.3, 3585.0)
	[12.7, 153.9, 166.7]	[586.3, 595.9, 1074.4, 1284.4, 1829.5, 3611.9]
	{12.7, 153.9, 166.7}	{569.2, 600.0, 1053.1, 1307.0, 1844.3, 3671.8}
TS1[c]	16.1, 236.1, 252.2	384.9***i***,239.3, 276.5, 798.3, 2141.9, 3812.7
	(5.49, 409.6, 415.1)	(58***i***, 132.7, 143.8, 401.8, 2224.9, 3723.2)
	[15.6, 232.5, 248.1]	[458.1***i***, 233.4, 271.7, 799.2, 2053.6, 3730.9]
	{15.6, 232.5, 248.1}	{389.1***i***, 105.4, 356.9, 815.2, 2085.6, 3818.9}
TS2[c]	8.1, 163.2, 171.3	2128.6***i***, 533.1, 653.9, 946.7, 1310.4, 2194.7
	(7.7, 164.1, 171.8)	(1536.1***i***, 537.0, 650.9, 920.0, 1310.8, 2207.5)
	[7.2, 163.4, 170.6]	[3180.5***i***, 570.9, 669.1, 981.4, 1371.5, 2155.5]
	{7.2, 163.4, 170.6}	{1626.2***i***, 646.6, 673.7, 1063.6, 1359.7, 2205.7}
TS3	9.1, 161.5, 170.6	1998.8***i***, 547.3, 680.9, 1147.1, 1887.5, 2247.8
	(9.1, 160.7, 169.8)	(1869.7***i***, 526.2, 679.6, 1153.7, 1856.6, 2137.6)
	[8.2, 162.8, 171.0]	[1770.5***i***, 529.7, 696.7, 1192.1, 1847.2, 2193.2]
	{8.2, 162.8, 171.0}	{1778.9***i***, 513.7, 677.4, 1145.9, 1864.9, 2182.6}

[a] For every intermediate or transition state, values from top to bottom are those obtained at QCISD/6-311G(d,p), B3LYP/6-311G(d,p), MP2/6-311G(d,p), and B3LYP/6-311G(d,p)//MP2/6-311G(d,p) levels, respectively. [b] The vibrational frequencies of Ar− or CO-matrix isolated trans-HOCO are 515, 615, 1065, 1211, 1844, and 3603 (cm^{-1}). Those of cis-HOCO are 620, 620, 1088, 1261, 1797, 3316 (cm^{-1}), Ref. (97). [c] The vibrational frequencies of TS1 calculated at CCSD(T)/6-311G(d,p) level are 343i, 197.7, 255.2, 752.9, 2127.4, and 3786.9 cm^{-1}. Those of TS2 are 2069.3**i,** 533.8, 643.5, 949.2, 1306.9, and 2177.6 cm^{-1}

TABLE 2: Vibrational Frequencies and Moments of Inertia of Some Key Intermediates and Transition States for the OD + CO Reaction Calculated at Various Levels[a]

species	I_a I_b I_c/au	ν_i /cm^{-1}
trans-DOCO[b]	11.8,168.9, 180.7	407.0, 602.4, 941.0, 1142.3, 1916.9, 2838.8
	(12.2, 186.7, 198.9)	(416.5, 577.3, 902.5, 1089.3, 1861.5, 2756.7)
	[11.8, 169.0, 180.9]	[411.5, 577.9, 907.4, 1114.67, 1848.7, 2744.5]
	{11.8, 169.0, 180.9}	{403.5, 594.1, 926.1, 1112.9, 1871.3, 2808.4}
cis-DOCO[b]	16.6, 157.4, 174.0	484.2, 557.9, 1008.6, 1171.6, 1882.4, 2718.3
	(16.7, 175.8, 192.5)	(498.3, 529.8, 949.6, 11342.2, 1834.3, 2590.1)
	[16.4, 158.1, 175.4]	[483.8, 540.5, 964.4, 1139.8, 1828.8, 2634.5]
	{16.4, 158.1, 175.4}	{500.0, 558.6, 996.7, 1177.9, 1890.0, 2722.7}
TS1	17.8, 248.6, 266.3	382.7***i***,184.5, 273.6, 586.3, 2141.5, 2776.0
	(8.1, 422.8, 430.9)	(57.4***i***, 102.9, 132.1, 290.3, 2224.7, 2719.1)
	[17.3, 244.7, 261.9]	[456.0***i***, 180.5, 269.0, 587.1, 2053.2, 2725.1]
	{17.3, 244.7, 261.9}	{387.5***i***, 140.6, 350.5, 605.8, 2085.2, 2789.6}
TS2	13.4, 171.5, 184.9	1694.2***i***,412.7, 618.3, 858.7, 1251.8, 2185.6
	(13.0, 192.8, 205.8)	(1208.9***i***, 409.1, 607.4, 822.8, 1197.9, 2165.3)
	[11.8, 171.7, 183.5]	[2564.8***i***, 442.9, 630.9, 904.5, 1280.5, 2138.8]
	{11.8, 171.7, 183.5}	{1315.8***i***, 520.6, 586.1, 921.2, 1282.0, 2197.2}
TS3	13.0, 164.9, 177.8	1469.7***i***, 472.9, 678.8, 1137.4, 1525.7, 1999.0
	(13.4, 183.9, 197.3)	(1370.9***i***, 452.2, 654.2, 1097.9, 1433.2, 1951.8)
	[12.1, 166.0, 178.1]	[1297.5***i***,457.6, 681.9, 1133.0, 1468.5, 1946.0]
	{12.1, 166.0, 178.1}	{1311.7***i***, 474.9, 675.1, 1122.9, 1484.2, 1998.9}

[a] For every intermediate or transition, values from top to bottom are those obtained at QCISD/6-311G(d,p), B3LYP/6-311G(d,p), MP2/6-311G(d,p), and B3LYP/6-311G(d,p)//MP2/6-311G(d,p) levels, respectively. [b] The vibrational frequencies of Ar− or CO-matrix isolated trans-DOCO are 472, 610, 1092, 1092, 1842, and 2558 (cm^{-1}). Those of cis-DOCO are 497, 563, 1148, 1148, 1798, 2456 (cm^{-1}), Ref. (97).

considered, these values affect the predicted rate constant significantly. In the following RRKM calculations, frequencies obtained by B3LYP//MP2/6-311G(d,p) are used.

3.2 PES and Reaction Mechanism. Our calculations indicate that the reaction of OH with CO proceeds mainly through the following two channels

$$\mathrm{OH} + \mathrm{CO} \rightarrow \text{vdw-OHCO} \xrightarrow{TS1} \textit{trans}\text{-HOCO}^{\dagger} \xrightarrow{+M} \mathrm{HOCO} \quad \text{(a)}$$

$$\textit{trans}\text{-HOCO}^{\dagger} \xrightarrow{TS5} \textit{cis}\text{-HOCO}^{\dagger} \xrightarrow{TS2} \mathrm{H} + \mathrm{CO_2} \quad \text{(b)}$$

$$\textit{trans}\text{-HOCO}^{\dagger} \xrightarrow{TS3} \mathrm{HCO_2}^{\dagger} \xrightarrow{TS4} \mathrm{H} + \mathrm{CO_2} \quad \text{(c)}$$

The potential energy profile drawn with the values obtained at the G2M level is presented in Figure 3 and the ZPE-corrected relative energies calculated at different levels of theory are summarized in Tables 3−5. As indicated above, the association reaction of OH and CO can directly form two weakly bound linear complexes, vdw-OHCO and vdw-OHOC. For vdw-OHCO, the computed ZPE-corrected dissociation energy D_0 are 1.4 and 1.3 kcal/mol at the G2M//B3LYP/6-311G(d,p) and G2M//MP2/6-311G (d,p) levels, respectively; these are in good agreement with the recent result of Lester et al., 1.23 kcal/mol.[94] For vdw-OHOC, D_0 are 0.8 and 0.7 kcal/mol predicted at the same levels of theory. When the zero-point energies calculated with the frequencies computed by B3LYP//MP2/6-311G(d,p) were used, D_0 for vdw-OHCO and vdw-OHOC were found to increase by about 0.5 and 0.3 kcal/mol, respectively, comparing with the values mentioned above.

As alluded to above, there are two stable reaction intermediates, i.e., *trans*-HOCO and *cis*-HOCO. Our results, summarized in Tables 3−5, give the dissociation energy D_0(HO−CO) = 24.1 and 23.9 kcal/mol for the *trans*-HOCO isomer, and the same value, 22.3 kcal mol^{-1}, for the *cis*-HOCO isomer by G2Q

TABLE 3: Relative Energies Calculated at Various Levels of Theory for OH +CO Reaction Based on G1 and G2 Methods[a]

		ΔE[b]				
species	ZPE[c]	QCISD	PMP4	QCISD(T)	G1	G2
OH + CO	5.4 (3.9), 3.1	0.0	0.0	0.0	0.0	0.0
H + CO_2	7.4	−17.8	−24.3	−21.5	−26.2	−25.1
Trans-HOCO	13.4 (11.2)	−16.1	−18.5	−18.2	−23.9	−24.1
Cis-HOCO	13.3 (11.2)	−14.9	−16.7	−16.9	−22.0	−22.3
HCO_2	12.4 (10.5)	−4.3	1.3	−2.1	−7.9	−7.5
TS1, OH + CO → trans-HOCO	10.4 (8.5)	5.1	3.9	3.5	1.0	1.3
TS2, cis-HOCO → H + CO_2	8.1 (7.6)	12.0	15.2	7.3	1.2	2.0
TS3, trans-HOCO → HCO_2	9.3 (8.3)	20.8	15.2	16.5	9.5	9.8
TS4, HCO_2 → H + CO_2	7.8 (7.4)	−0.9	−6.9	−3.8	−10.5	−9.7
TS5, trans-HOCO → cis-HOCO	12.3 (10.3)	−8.0	−9.9	−10.0	−15.7	−15.8

[a] All values relative to OH + CO are in units of kcal/mol. [b] Zero-point energies (ZPE) are included in the relative energies. [c] The values in parentheses are for those of the OD + CO reaction.

TABLE 4: Relative Energies for OH(D) + CO Reactions at the G2M Level Based on Different Optimized Geometries

	ZPE (kcal/mol)			ΔE (kcal/mol)		
species	B3LYP[a]	MP2[b]	B3LYP// MP2[c]	G2M[a]// B3LYP	G2M // MP2[b]	G2M/// B3LYP//MP2[c]
OH + CO	8.5	8.6	8.5 (7.0)	0.0	0.0	0.0
H + CO_2	7.4	7.3	7.3	−24.6	−24.7	−24.7
Vdw-OHOC	9.1	9.3	8.9 (7.4)	−0.8	−0.7	−1.0 (−1.0)
Vdw-OHCO	9.4	9.5	9.0 (7.5)	−1.4	−1.3	−1.8 (−1.6)
Trans-HOCO	13.4	13.4	13.1 (11.0)	−23.9	−23.7	−23.9 (−24.5)
Cis-HOCO	13.3	13.3	12.9 (10.0)	−22.3	−22.0	−22.3 (−22.7)
HCO_2	12.4	12.5	11.2 (9.4)	−9.6	−7.7	−9.0 (−9.2)
TS1, OH + CO → trans-HOCO	10.4	10.4	10.3 (8.4)	0.3	0.9	0.8 (0.5)
TS2, cis-HOCO → H + CO_2	8.1	8.5	8.5 (8.0)	2.8	2.2	2.3 (3.1)
TS3, trans-HOCO → HCO_2	9.3	9.5	9.1 (8.2)	10.4	10.7	10.7 (11.3)
TS4, HCO_2 → H + CO_2	7.8	8.1	7.9 (7.4)	−9.4	−8.1	−9.4 (−8.5)
TS5, trans-HOCO → cis-HOCO	12.3	12.3	12.0 (10.1)	−15.7	−15.3	−15.6 (−15.9)
TS6, vdw-OHOC → vdw-OHCO	9.1	8.9	8.9 (7.4)	0.02	−0.2	−0.1 (−0.1)

[a] G2M energies are calculated based on the structures optimized at B3LYP/6-311G (d, p) level and the zero- point energies (ZPE) in this level are included in the relative energies. [b] G2M energies are calculated based on the structures optimized at MP2/6-311G(d, p) level and the zero-point energies (ZPE) in this level are included in the relative energies. [c] The values in parentheses are for those of the OD + CO reaction; the ZPE, calculated at B3LYP//MP2/6-311G(d, p) level, are included in G2M energies.

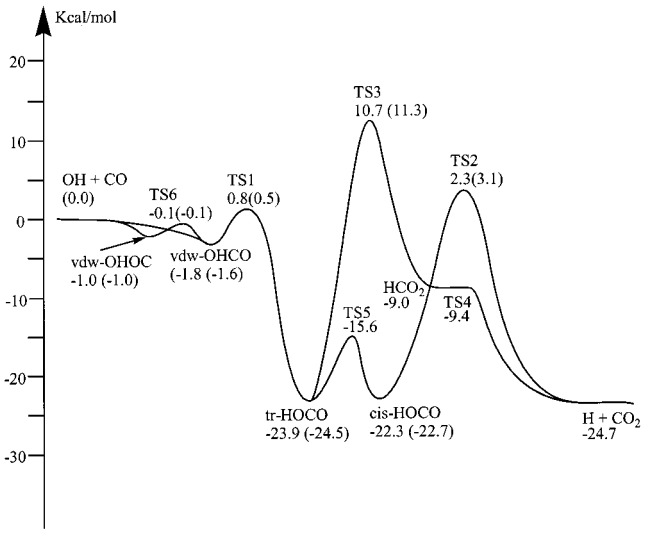

Figure 3. Potential energy surface for the OH(OD) + CO reactions based on ab initio prediction. The values given in the figure are from G2M calculations with ZPE-corrected. Those in parentheses are for the OD + CO reaction with the same level of theory.

and G2M, respectively. The present results agree well with the recent experimental value of Ruscic and Litorja[52(b)], 24.1 kcal/mol (for *cis*- or *trans*-isomer) and those of Duncan and Miller,[98] 25.4 and 24.3 kcal/mol for *trans*-HOCO and 23.4 and 22.4 kcal/mol for *cis*-HOCO calculated at the CBS-QB3 and G3 levels of theory, respectively. Fulle et al.[39] obtained the D_0 to be 30.8 kcal/mol from their kinetic data analysis. The values obtained by Aoyagi and Kato[73] were 16.9 *trans*-HOCO and 15.5 kcal/mol for *cis*-HOCO; they added 9.0 kcal/mol to correct the dissociation energy in their calculations for the rate constant. The isomerization barrier between *cis*- and *trans*-HOCO are predicted to be 6.5 and 6.7 kcal/mol at the G2Q and G2M levels, comparing with the values of 6.1 and 6.2 kcal/mol calculated at the CBS-QB3 and G3 levels by Duncan and Miller.[98] The above comparison indicates that for the dissociation energy of HOCO, the difference between theory and experiment is narrowing, although there is still room for further improvement. However, for the rate coefficient prediction, the result depends less sensitively on the HO−CO dissociation energy than on the barrier heights at TS1 and TS2.

For channel (b), because of the importance of TS1 and TS2 for rate constant calculations, we investigated these two transition states in greater detail and compared them with the data available in the literature. Our results indicate that the barrier at TS1 predicted by different levels of theory varies from 0.3 to 1.5 kcal/mol, with the average value of 1.0 ± 0.3 kcal/mol based on the optimized structures at B3LYP/6-311G(d,p), MP2/6-311G(d,p), MP2/6-311++G(d,p), B3LYP/6-31G(2d,2p), and CCSD(T)/6-311G(d,p) levels (see Tables 3−5). The G1 and G2 methods predict the TS1 barrier to be 1.0 and 1.3 kcal mol^{-1} based on the QCISD/6-311G(d, p) structure. These are to be compared with that of Schatz et al., 3.7 kcal/mol at the SDCI/DZP level of theory.[64] Their value was reduced to −0.9 kcal/mol^{-1} (based on an RRKM estimate) for the purpose of quasiclassical trajectory calculations.[63(a)] Similarly, Aoyagi and

TABLE 5: Comparison of the Relative Energies for the OH + CO Reaction[a] by Different Authors

species	Schatz et al.[b] (ref 63)	Aoyagi et al.[c] (ref 73)	Duncan et al. (ref 100)	this work G2Q	this work G2M[d]	exp. Ref(52, 100)
H+CO2	−18.5(−23.5)	−13.2(−22.2)	−25.0(−24.9)	−25.1	−24.7	−24.3
Vdw-OHCO					−1.8	
Vdw-OHOC					−1.0	
Trans-HOCO	−22.4(−36.9)	−16.9(−25.9)	−25.4(−24.3)	−24.1	−23.9	−27.8 (−24.4)
Cis-HOCO	−21.0(−35.7)	−15.5(−24.5)	−23.4(−22.4)	−22.3	−22.3	
HCO2	−10.6(−27.0)			−7.5	−9.0	−11.4
TS1	3.7(−0.9)	2.9		1.3	0.8[e]	
TS2	12.5(2.5)	18.4(9.4)	1.1 (0.0)	2.0	2.3[e]	
TS3	18.7(6.5)			9.8	10.7	
TS4	−0.2(−10.8)			−9.7	−9.4	
TS5	−27.7		−17.3(−16.2)	−15.8	−15.6	

[a] All values are in units of kcal mol^{-1}, relative to the OH + CO reactants (including ZPE corrections). [b] Values adapted from ref. (63), those in parentheses are from their "best estimate". [c] Values adapted from ref. (73), the modified results are shown in parentheses. [d] The ZPEs obtained at B3LYP/6-311G(d,p)//MP2/6-311G(d,p) level are included in G2M energies. [e] On the basis of the optimized geometries at B3LYP/6-311G(d, p), MP2/6-311G(d, p), MP2/6-311++G(d, p), B3LYP/6-311G(2d, 2p) and CCSD(T)/6-311G(d, p), the G2M energies for TS1 are 0.3, 0.9, 0.9, 1.4 and 1.5 kcal/mol, those of for TS2 are 2.8, 2.6, 2.7, 2.8 and 2.6 kcal/mol, respectively.

Kato[73] obtained a barrier height of 2.9 kcal/mol for TS1 with a multireference method carried out at the MRD-CI/DZP level of theory. Very recently, Lester et al.[94] reported the TS1 barrier to be 1.1 kcal/mol at the CCSD(T)/aug-cc-pvtz level and Duncan and Miller[98] reported that the barrier was negligible at the CBS-QB3 and G3 levels based on the structures optimized at the B3LYP/6-311++G(3df,3pd) level of theory. The TS2 barrier also appears to be scattered, calculating at different levels of theory (see Tables 3−5). In our calculations, the G2M values for TS2 (relative to OH + CO) vary very slightly using the structures optimized with different methods: 2.8, 2.6, 2.7, 2.8 and 2.6 kcal/mol, respectively, based on G2M//B3LYP/6-311G-(d,p), G2M//MP2/6-311G(d,p),G2M//MP2/6-311+G(d,p), G2M//B3LYP/6-31G(2d,2p), and G2M//CCSD(T)/6-311G(d,p). When the ZPE-correction was made with the frequencies calculated by B3LYP//MP2/6-311G(d,p), it becomes 2.3 kcal/mol. At the G2Q level, it is 2.0 kcal/mol. These values are much smaller than the TS2 barrier obtained by Schatz et al.,[64] 12.5 kcal/mol; however, they estimated the "best value" to be 2.5 kcal/mol from RRKM calculations. In Aoyagi and Kato's calculation,[73] the barrier was 18.4 kcal/mol and the modified value for their RRKM calculations was 9.4 kcal/mol. Duncan and Miller[98] predicted the TS2 barrier to be 1.1 and 0.0 kcal/mol by CBS-QB3 and G3, respectively. From the above comparison, we can conclude that the barrier height of TS2 is larger than that of TS1 if the same method is used. Therefore, hydrogen elimination from *cis*-HOCO, is expected to occur significantly by tunneling through TS2.

For channel (c), to reach HCO_2 the reaction has to proceed via TS3, which involves a 1,2-H shift with a much higher barrier as the rate-controlling step; it is kinetically unimportant.

Finally, the enthalpy of the reaction at 0 K is predicted to be −24.6, −24.7, and −25.1 kcal/mol, respectively, at the G2M//B3LYP/6-311G(d,p), G2M//MP2/6-311G(d,p) and G2//QCISD/6-311G(d,p) levels of theory. These values are consistent with the results of −24.5 and −25.0 kcal/mol predicted at G3 and CBS-QB3 levels[100] and are in excellent agreement with the experimental values (−24.5 kcal mol^{-1} at 0 K).[52(b),99]

3.3 Rate Constant Calculations. As aforementioned, the rate constants for the OH(OD) + CO reactions were evaluated by the Variflex code[75] using the energies plotted in Figure 3 and the frequencies listed in Tables 1 and 2, with a minor adjustment in the barrier at TS2 to account for the T,P-effects on the overall rate coefficients over a wide range of conditions.[100] For the association of OH + CO to vdw-OHCO process, a Morse potential with $\beta = 1.53$ A^{-1} and $D_e = 2.2$ kcal/mol were used, the effect of multiple reflections above the well of the vdw-OHCO complex was calculated with the method of Wigner and Hirschfelder,[101,102] the effect was found to be negligible. Therefore, in all subsequent calculations, we ignored the effect of the vdw-complexes on the total rate constant. The rate constant was calculated with 0.8 kcal/mol barrier at TS1 and 2.0, instead of 2.3 kcal /mol, at TS2, to mach almost all existing, reliable rate constants as functions of P and T. For a more reliable prediction of the pressure effect, the Lennard−Jones (L−J) potential for the He−HOCO system, as shown in Figure 4, was calculated by MP2/6-311+G(3df, 2p). The ϵ and σ parameters for the He−HOCO system were determined to be 51 K and 3.5 Å by fitting the potential to the L−J function,[103] $V(r) = 4\epsilon\,[(\sigma/r)^{12} - (\sigma/r)^6]$. These parameters could then be de-convoluted and convoluted with the L−J parameters of pure buffer gases taken from the literature:[104] $\sigma = 2.55$, 3.47, 3.74, 4.40, and 5.20 Å; $\epsilon/\kappa = 10$, 114, 82, 166, and 212 K for He, Ar, N_2, CF_4, and SF_6 , respectively, using the approximation, $\sigma_{12} = (\sigma_1+\sigma_2)/2$; $\epsilon_{12} = (\epsilon_1\epsilon_2)^{1/2}$ for each collision pair.

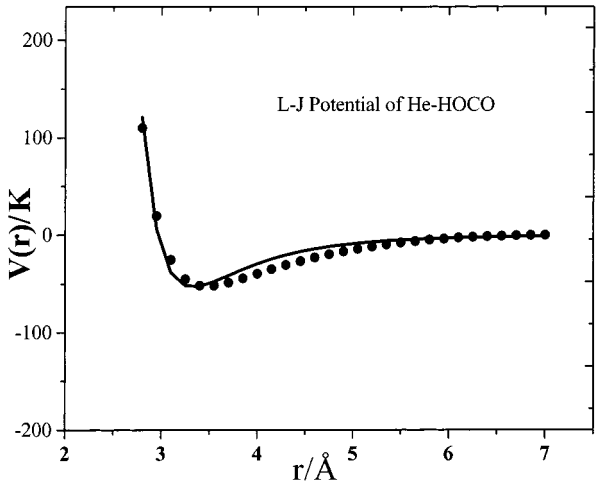

Figure 4. L−J potential energy curve for HOCO−He calculated at the MP2/6-311+G(3df, 2p) level. Solid circles are calculated data and the curve is the fitting result with $\sigma = 3.5$ Å and $\epsilon/k = 51$.

Table 6 lists the L−J parameters and the average energy removed per collision by the third-body, $\langle\Delta E\rangle_{down}$, from the excited HOCO intermediate. The $\langle\Delta E\rangle_{down}$ values were obtained by comparing the experimental pressure-dependent rate constants k_{tot},[8,16,21,39] with the calculated values using the

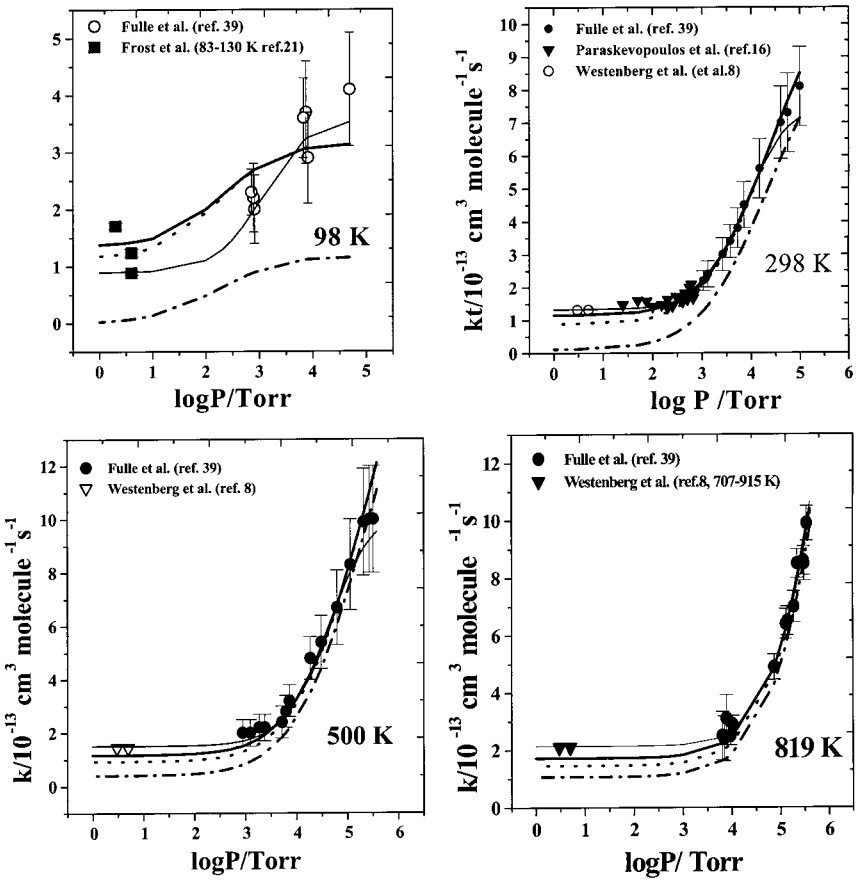

Figure 5. Pressure dependence of total rate constant with and without tunneling effect (M=He) at different temperature. The symbols are from direct kinetic measurements as labeled in the legend and the curves are the RRKM results; solid curves are the results from 2.0 kcal/mol for TS2 with tunneling corrections, dotted curves are those with 2.3 kcal/mol for TS2 (with tunneling) and the dash−dotted curves are those with 2.0 kcal/mol for TS2 without tunneling corrections. The thinner lines are the fitting results of ref 39.

TABLE 6: Lennard−Jones Parameters and $<\Delta E>_{down}$ Values Used in RRKM Calculations for Various HOCO−M Collision Partners

M	σ/Å	ϵ/K	$<\Delta E>_{down}$/cm^{-1}
He	3.5	51	150
N_2	4.0	146	250
Ar	3.8	174	400
CF_4	4.3	208	450
SF_6	4.7	235	1000

exponential-down model in the solution of the master equation. Our $<\Delta E>_{down}$ value obtained by the modeling for He, 150 cm^{-1}, is the same as that employed by Fulle[39] and co-workers and the value for N_2, 250 cm^{-1}, can be compared with the averaged step-size used by Golden et al.,[50] 210 cm^{-1}. The L−J parameters employed by Fulle et al. for He and HOCO gave $\sigma_{He-HOCO} = 3.3$ Å and $\epsilon_{He-HOCO} = 45$ K, which are close to our values given above derived from ab initio calculations.

A. Pressure Effect. The OH + CO reaction was found to be strongly pressure dependent.[8,16,17,21,39,50,105] Figure 5 shows the rate coefficients measured at different temperatures for the reaction as a function of helium pressure. The solid curves are the results of calculations using 2.0 kcal/mol for the TS2 barrier and the dotted ones are those predicted with 2.3 kcal/mol instead; tunneling effects are included. The dash−doted curves are those obtained with 2.0 kcal/mol for TS2 barrier without tunneling corrections. The thinner solid lines are the fitting results of Fulle et al.[39] The results are in good agreement with experimental data[8,21,39] either at low temperature and low pressure or high temperature and high pressure when the tunneling effect is considered in the calculations. The high-pressure rate constants (see Table 7) at different temperatures are close to the experimental and fitting values from the work of Fulle et al.[39] Take some temperatures for example; k^∞ at 100, 200, 300, 500, and 800 K predicted by our calculations are 3.23, 7.15, 11.3, 19.2, and 35.8 × 10^{-13} cm^3 molecule^{-1}s^{-1}, respectively, which compare closely with the fitting values[39] of 4.0, 7.0, 9.6, 16.2, and 30 × 10^{-13} cm^3 molecule^{-1}s^{-1} at 98, 190, 300, 500, and 819 K, respectively, and the values of 12.0 and 15.0 × 10^{-13} cm^3 molecule^{-1}s^{-1} at 314 and 512 K, inferred from measurements of the rate constants for the relaxation of OH(v=1) by CO.[39]

One of the goals in the present study is to model the effect of pressure on OH + CO by various third bodies through solution of the master equation. To our knowledge, five groups[12,15,16,19,22] have performed extensive studies on the reaction in the presence of different buffer gases, such as He, Ar, N_2, Air, CF_4, and SF_6. The third-body effect on k_{tot} was found to be significant, especially for those which have greater internal degrees of freedom (e.g., CF_4 and SF_6) for quenching of the excited intermediate. Figures 6 (a)−(d) show the modeled k_{tot} in comparison with experimental results at 298 K for various third bodies, M = Air, N_2, CF_4, and SF_6, respectively (dotted curves are the results obtained with 2.3 kcal/mol TS2 barrier and the solid curves are those with 2.0 kcal/mol barrier). These results suggest that the stabilization of HOCO† by collisional deactivations is significant for the third-bodies with high collisional efficiencies (e.g., SF_6 and CF_4) at moderate and high pressures and the dissociation of HOCO† forming the CO_2 product via TS2 would be dominant for the third-bodies with weak-collision efficiencies (e.g., He or Ar) at low and medium

TABLE 7: Calculated Rate Coefficients and S/D Ratios for the Reaction of OH with CO at Selected Temperatures and Pressures with Ar as Buffer Gas.[a,b]

	5 Torr			100 Torr			1 atm			10 atm			∞
T/K	k_{tot}	*S*	*D*	k_{tot}	*S*	*D*	k_{tot}	*S*	*D*	k_{tot}	*S*	*D*	k_{tot}
20	0.1	0.61	0.39	0.1	0.97	0.03	0.1	1.0	0.0	0.1	1.0	0.0	0.1
40	0.69	0.60	0.40	0.75	0.94	0.06	0.76	0.99	0.01	0.76	1.0	0.0	0.76
60	1.20	0.25	0.75	1.47	0.90	0.10	1.54	0.99	0.01	1.55	1.0	0.0	1.55
80	1.45	0.16	0.84	2.04	0.85	0.15	2.31	0.98	0.02	2.39	1.0	0.0	2.39
100	1.53	0.10	0.90	2.37	0.79	0.21	2.97	0.96	0.04	3.19	1.0	0.0	3.23
200	1.29	0.01	0.99	1.97	0.45	0.55	3.60	0.85	0.15	5.90	0.97	0.03	7.15
300	1.22	0.01	0.99	1.54	0.22	0.78	2.72	0.67	0.33	6.03	0.93	0.07	11.3
500	1.20	0.01	0.99	1.28	0.07	0.93	1.70	0.34	0.66	3.80	0.76	0.24	19.2
800	1.90	0.0	0.99	1.93	0.0	0.99	2.00	0.04	0.95	2.54	0.27	0.72	35.8
1000	2.22	0.0	0.98	2.24	0.0	0.98	2.26	0.01	0.97	2.49	0.12	0.87	45.5
1500	4.45	0.0	0.94	4.45	0.0	0.94	4.45	0.0	0.94	4.47	0.0	0.94	86.1
2000	8.02	0.0	0.90	8.02	0.0	0.90	8.02	0.0	0.90	8.02	0.0	0.90	140.
2500	13.0	0.0	0.85	13.1	0.0	0.85	13.1	0.0	0.85	13.1	0.0	0.85	207.
3000	19.8	0.0	0.81	19.8	0.0	0.81	19.8	0.0	0.81	19.8	0.0	0.81	287.

[a] Rate coefficients are in units of 10^{-13} cm^3 molecule^{-1}s^{-1}. [b] $S = k_a/k_{tot}$; $D = k_b/k_{tot}$; $k_{tot} = k_a + k_b + k_c$.

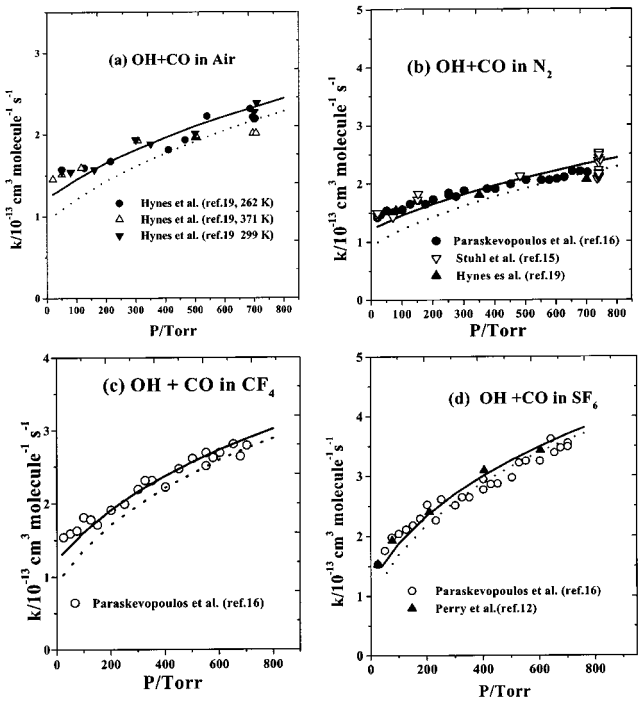

Figure 6. Pressure dependence of the total rate constant with various third bodies for the OH + CO reaction. (a) Air, (b) N_2, (c) CF_4, and (d) SF_6. The symbols are from direct kinetic measurements as labeled in the legends and the curves are the RRKM results at 298 K.

pressures. Figures 7 (a) and (b) show the predicted k_{tot} in comparison with experimental results of OD + CO reaction for M = N_2 and CF_4, respectively. The rate constant was calculated with 0.5 kcal/mol barrier at TS1 and 2.8 kcal/mol at TS2.

B. Temperature Effects. The Arrhenius plots of the OH + CO reaction for M = Ar are shown in Figure 1 (a) and Figure 1(b). The RRKM results are drawn as curves in the plots for the pressure at 5 Torr, with and without tunneling corrections, to illustrate the effect of tunneling corrections. The results shown for 10 Torr, 100 Torr, 1 and 10 atm were all obtained with tunneling corrections. The fitting result of Fulle et al.[39] for 5 Torr He and the data of Golden et al.[50] for 1.3−2.6 atm in Ar are also plotted for comparison. The plots show that at lower temperatures, the fitting result of Fulle and our predicated value are consistent within experimental scatters; however, Fulle's curve-fitting result is seen to deviate at high temperatures from

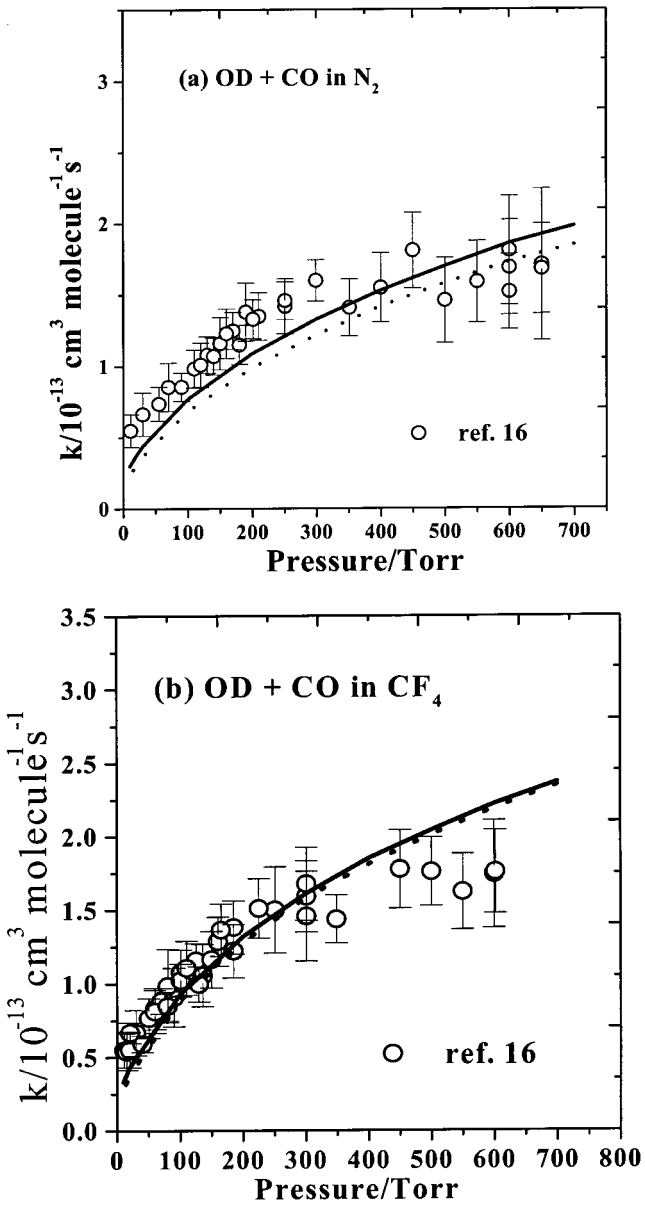

Figure 7. Pressure dependence of the total rate coefficient with various third bodies for OD + CO reaction. (a) N_2, (b) CF_4. Points from ref 16 and curves are the predicted values at 298 K. Solid and dotted curves represent values computed with 2.8 and 3.1 kcal/mol barrier at TS2, respectively.

our predicted value, which agrees with the majority of experimental data as discussed below.

The theoretical results clearly indicate the significant effects of temperature, pressure and tunneling. The total rate constants and the stabilization and decomposition ratios (relative to k_{tot}) are tabulated in Table 7 for P(Ar) = 5 Torr, 100 Torr, 1 atm, 10 atm and the high-pressure limit at thirteen temperatures between 20 and 3000 K. The results shown in Figure 1 and Table 7 reveal that k_{tot} is almost temperature-independent at low pressures (5 Torr) in the temperature range of 60−500 K, which is in good agreement with the experimental results of Frost et al.;[21] however, at lower temperatures, for example at T = 20 K, the rate constant (at 5 Torr) decreases by one order, compared to those between 60 and 500 K, consistent with the prediction of Smith.[21 (c)] The comparison of our RRKM result with high-temperature experimental data is illustrated in the Figure 1 (b). The predicted value is in good agreement with the flame modeling results of Vandooren et al.[34] and the shock tube data of Wooldridge et al.[35] and Golden et al.[50] under combustion conditions. This comparison indicates a good agreement between theory and experiment over a wide range of temperautres, reflecting the reasonableness of the ab initio data (especially for TS1 and TS2) used in the present RRKM calculations.

C. Effect of the Re-dissociation of the Thermalized HOCO. The present calculations predict the rate constants for the production of CO_2 and the stabilization of HOCO under initial reaction conditions, ignoring the effect of the reactivation/re-dissociation of the thermalized HOCO in the duration of the OH decay kinetic measurement. To test such an effect, we have carried out kinetic modeling for OH decay rates under the atmospheric condition between 500 and 1500 K, including the predicted bimolecular processes producing HOCO and H + CO_2, the re-dissociation reactions (HOCO + M→ OH + CO + M and HOCO + M → H + CO_2 + M), as well as the removal of HOCO by reactions with H and OH. The result of the kinetic modeling indicates that the effect of the re-dissociation of thermalized HOCO on OH decay rates amounts to less than 1% under the atmospheric pressure condition. At the highest pressure studied by Fulle et al.[39] at 819 K, $P = 4.1 \times 10^5$ Torr, under which the re-dissociation effect is expected to be most significant, the predicted effect on OH decay is about 25%. The effect was found to decrease at temperatures higher than 1000 K due to the increased energy to overcome the TS2 barrier. At lower temperatures, the consumption of HOCO by H and OH (which were assumed to have the same rate constants as HCO reactions with H and OH) also reduced the effect on OH decay rates. Under the conditions of interest to practical high-temperature combustion or low-temperature atmospheric chemistry, the effects of the re-dissociation of the thermalized HOCO can, therefore, be ignored.

D. Kinetic Isotope and Tunneling Effects. Paraskevopoulos et al.[16] measured the rate constant for OD + CO at room temperature and found that this rate constant was about one-third of that for OH + CO. This also suggests that the effect of tunneling is important at low temperatures. Theoretically, several groups,[21,39,50,73] have reported the importance of the tunneling effect, but different results were predicted. For example, in Aoyagi and Kato's calculation, they found a strong tunneling effect and they attributed this to the greater barrier of TS2 (5.6 kcal/mol) than that of TS1 (1.3 kcal/mol). However, the calculation of Fulle et al.[39] suggested that tunneling contribution was negligible because the imaginary frequency used in their calculations was only 239 cm^{-1} for the H + CO_2 production,

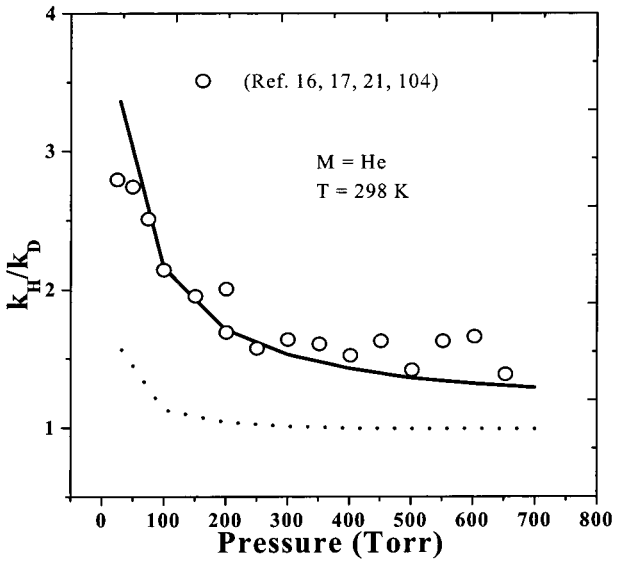

Figure 8. Comparison of the RRKM prediction with the experimental results (symbols) for the kinetic isotope effect (k_H/k_D) as a function of pressure reported in refs 16, 17, 21, and 104. The solid and dotted curves are the results of calculations with and without tunneling corrections.

considerably lower than the predicted imaginary frequency for TS2 (ranging from −1500 to −3300 cm^{-1} at different levels of theory). Golden et al.[50] also reported that no tunneling correction was required in their RRKM modeling because their exit barrier was assumed to lie below the entrance channel; however, they also pointed out that it was not possible to fit the low-temperature kinetic data without including tunneling corrections. It is evident from Figures 1, 5 and 8 that the effect of tunneling on this reaction is very significant, especially under low-pressure and low-temperature conditions when the population of $HOCO^\dagger$ is peaking near TS2.

The overall kinetic isotope effect has also been examined in terms of the k_H/k_D ratio as a function of pressure (see Figure 8 for M = He). The symbols in the figure represent the experimental results of various groups[16,17,21,104] and the curves for different pressures as indicated is from our RRKM calculations. The theoretical results agree reasonably with the experimental data when the effect of tunneling is included.

4. Conclusion

We have studied theoretically the effects of temperature, pressure, and quantum-mechanical tunneling on the kinetics of the OH(D) + CO reactions. The rate constants for the reactions have been predicted with a multichannel RRKM calculation employing the potential energy surface data obtained by the G2-type methods. The absolute values of the total rate constant were found to be affected strongly by the barrier heights at TS1 and TS2 and independent of the weakly bound van der Waals intermediates OHOC and OHCO. The barriers at TS1 and TS2 were found to converge to 1.0 and 2.3 kcal/mol, respectively, from various recent calculations with about 1 (or ± 0.5) kcal/mol spread in the predicted values. Experimental data could be best accounted for with 0.8 and 2.0 kcal, using the 1626 cm^{-1} imaginary frequency for tunneling corrections. The use of a larger imaginary frequency could make the 0.3 kcal/mol reduction in the barrier at TS2 unnecessary.

The experimentally observed strong non-Arrhenius behavior of the bimolecular rate constants for both reactions was found to result from the combination of temperature, pressure, and

quantum-mechanical tunneling. The combined effect of the latter two factors at low temperatures gives rise to the significant leveling-off of the rate constants below 1000 K. The sharp increase in the rate constant above 1000 K was found to result from the rapid increase in the vibrational partition function associated with CO_2 production and the disappearance of the effect of tunneling. The experimentally measured large, pressure-dependent isotope effect (k_H/k_D) can also be reasonably accounted for by the combination of *T*, *P*, and tunneling effects.

Acknowledgment. This work was supported in part by the Basic Energy Sciences, Department of Energy under grant no. DE-FG05-91-ER14192 (to EWGD) and in part by ONR under grant no. N00014-89-J-1949 (to RZ, M.C.L. and A.M.M.). We also acknowledge Dr. D. Chakraborty for his confirmation on the existence of the van der Waals complex, OHCO, in 1999.

References and Notes

(1) Gardiner, W. C., Jr., Ed. *Combustion Chemistry*; Springer-Verlag: New York, 1986.

(2) Glassman, I. *Combustion*, 2nd ed.; Academic Press: Orlando, 1987.

(3) Wayne, R. P. *Chemistry of Atmospheres*, 2nd ed.; Clarendon Press: Oxford, 1991.

(4) Baulch, D. L.; Cobos, C. J.; Cox, R. A.; Esser, C.; Frank, P.; Just, Th.; Kerr, J. A.; Pilling, M. J.; Troe, J.; Walker, R. W.; Warnatz, J. *J. Phys. Chem. Ref. Data* **1992**, *21*, 566.

(5) Dixon-Lewis, G.; Wilson, W. E.; Westenberg, A. A. *J. Chem. Phys.* **1966**, *44*, 2877.

(6) Greiner, N. R. *J. Chem. Phys.* **1969**, *51*, 5049.

(7) Stuhl, F.; Niki, H. *J. Chem. Phys.* **1972**, *57*, 3671.

(8) Westenberg, A. A. deHaas, N. *J. Chem. Phys.* **1973**, *58*, 4061.

(9) Smith, I. W. M.; Zellner, R. *J. Chem. Soc., Faraday Trans. 2* **1973**, *69*, 1617.

(10) Howard, C. J.; Evenson, K. M. *J. Chem. Phys.* **1974**, *61*, 1943.

(11) Davis, D. D.; Fischer, S.; Schiff, R. *J. Chem. Phys.* **1974**, *61*, 2213.

(12) Perry, R. A.; Atkinson, R.; Pitts, J. N., Jr. *J. Chem. Phys.* **1977**, *67*, 5577.

(13) Clyne, M. A. A.; Holt, P. M. *J. Chem. Soc., Faraday Trans. 2* **1979**, *75*, 569.

(14) Ravishankara, A. R.; Thompson, R. L. *Chem. Phys. Lett.* **1983**, *99*, 377.

(15) Stuhl, F.; Hofzumahaus, A. *Ber. Bunsen-Ges. Phys. Chem.* **1984**, *88*, 557.

(16) (a) Paraskevopoulos, G.; Irwin, R. S. *J. Chem. Phys.* **1984**, *80*, 259. (b) Paraskevopoulos, G.; Irwin, R. S. *Chem. Phys. Lett.* **1982**, *93*, 138.

(17) Jonah, C. D.; Mulac, W. A.; Zeglinski, P. *J. Phys. Chem.* **1984**, *88*, 8, 4100.

(18) Beno, M. F.; Jonah, C. D.; Mulac, W. A. *Int. J. Chem. Kinet.* **1985**, *17*, 1091.

(19) Hynes, A. J.; Wine, P. H.; Ravishankara, A. R. *J. Geophys. Res.* **1986**, *91*, 11815.

(20) Brunning, J.; Derbyshire, D. W.; Smith, I. W. M.; Williams, M. D. *J. Chem. Soc., Faraday Trans. 2* **1988**, *84*, 105.

(21) (a) Frost, M. J.; Sharkey, P.; Smith, I. W. M. *Faraday Discuss. Chem. Soc.* **1991**, *91*, 305. (b) Frost, M. J.; Sharkey, P.; Smith, I. W. M. *Faraday Discuss. Chem. Soc. J. Phys. Chem.* **1993**, *97*, 12 254. (c) Smith, I. W. M., Mon. Not. R. Astron. Soc. **1998**, *234*, 1059.

(22) Forster, R.; Frost, M. J.; Fulle, D.; Hamann, H. F.; Hippler, H.; Schlepegrell, A.; Troe, J. *J. Chem. Phys.* **1995**, *103*, 2949.

(23) (a) Fenimore, C. P.; Jones, G. W. *J. Phys. Chem.* **1958**, *62*, 1578. (b) Fenimore, C. P.; Jones, G. W. *J. Chem. Phys.* **1963**, *39*, 1514.

(24) Hottel, H. C.; Williams, G. C.; Nerheim, N. M.; Schneider, G. R. *10th Symp. (Intl.) on Combustion, [Proc.]*; The Combustion Institute: Pittsburgh, PA, 1964; p 129.

(25) Westenberg, A. A.; Fristrom, R. M. *10th Symp. (Intl.) Combustion [Proc.]*; The Combustion Institute: Pittsburgh, PA, 1964; p 473.

(26) Dixon-Lewis, G.; Sutton, M. M.; Williams, A. *10th Symp. (Intl.) Combustion* [Proc.]; The Combustion Institute: Pittsburgh, PA, 1964; p 495.

(27) Porter, R. P.; Clark, A. H.; Kaskan, W. E.; Browne, W. E. *11th Symp. (Intl.) Combustion [Proc.]*; The Combustion Institute: Pittsburgh, PA, 1966; p 907.

(28) Heath, G. A.; Pearson, G. S. *11th Symp. (Intl.) Combustion [Proc.]*; The Combustion Institute: Pittsburgh, PA, 1966; p 967.

(29) Wilson, W. E., Jr.; O'Donovan, J. T.; Fristrom, R. M. *12th Symp. (Intl.) Combustion [Proc.]*; The Combustion Institute: Pittsburgh, PA, 1968; p 929.

(30) (a) Baldwin, R. R.; Walker, R. W.; Webster, S. J. *Combust. Flame* **1967**, *15*, 167; (b) Atri, G. M.; Baldwin, R. R.; Jackson, D.; Walker, R. W. *Combust. Flame* **1977**, *30*, 1.

(31) Dryer, F.; Naegeli, D.; Glassman, I. *Combust. Flame* **1971**, *17*, 270.

(32) Peeters, J.; Mahnen, G. *14th Symp. (Intl.) Combustion [Proc.]*; The Combustion Institute: Pittsburgh, PA, 1972; p 133.

(33) Eberius, K. H.; Hoyermann, K.; Wagner, H. Gg. *14th Symp. (Intl.) Combustion [Proc.]*; The Combustion Institute: Pittsburgh, PA, 1972; p 147.

(34) Vandooren, J.; Peeters, J.; Tiggelen, P. J. V. *15th Symp. (Intl.) Combustion [Proc.]*; The Combustion Institute: Pittsburgh, PA, 1974; p 745.

(35) Wooldridge, M. S.; Hanson, R. K.; Bowman, C. T. *25th Symp. (Intl.) Combustion [Proc.]*; The Combustion Institute: Pittsburgh, PA, 1994; p 741.

(36) Izod, T. P. J.; Kistiakowsky G. B.; Matsuda, S. *J. Chem. Phys.* **1971**, *55*, 4425.

(37) Brabbs, T. A.; Belles, F. E.; Brokaw, R. S. *13th Symp. (Intl.) Combustion [Proc.]*; The Combustion Institute: Pittsburgh, PA, 1970; p 129.

(38) (a) Gardiner, W. C.; Jr.; Mallard, W. G.; McFarland, M.; Morinaga, K.; Owen, J. H.; Rawlins, W. T.; Takeyama, T.; Walker, B. F. *14th Symp. (Intl.) Combustion [Proc.]*; The Combustion Institute: Pittsburgh, PA, 1972; p 61. (b) Lissianski, V.; Yang, H.; Qin, Z.; Mueller, M. R.; Shin, K. S.; Gardiner, W. C., Jr. *Chem. Phys. Lett.* **1995**, *240*, 57.

(39) Fulle, D.; Hamann, H. F.; Hippler, H. and Troe, J. *J. Chem. Phys.* **1996**, *105*, 983.

(40) Trainor, D. W.; Rosenberg, C. W., Jr. *Chem. Phys. Lett.* **1974**, *29*, 35.

(41) Biordi, J. C.; Lazzara, C. P.; Papp, J. F. Symp. Int. Combust. Proc. **1975**, *15*, 917.

(42) Gordon, S.; Mulac, W. A. *Int. J. Chem. Kinetic. (Symp. 1)* **1975**, 289.

(43) DeMore, W. B.; Golden, D. M.; Hampson, R. F.; Howard, C. J.; Kurylo, M. J.; Molina, J.; Ravishankara, A. R.; Sander, S. P. Chemical Kinetics and Photochemical Data for use in Stratospheric Modeling Evaluation No.8, JPL Publication 87-411987, 1.

(44) Zellner R. *J. Phys. Chem.* **1979**, *83*, 18.

(45) Dean, A. M.; Kistiakowsky, G. B. *J. Chem. Phys.* **1970**, *54*, 1718.

(46) DeMore, W. B. *Int. J. Chem. Kinet*. **1984**, *16*, 1187.

(47) Troe, J. *Ber. Bunsen-Ges. Phys. Chem.* **1994**, *98*, 1399.

(48) Mozurkewich, M.; Lamb, J. J.; Benson, S. W. *J. Phys. Chem.* **1994**, *88*, 6435.

(49) Larson, C. W.; Stewart, P. H.; Golden, D. M. *Int. J. Chem. Kinet.* **1988**, *20*, 27.

(50) Golden, D. M.; Smith, G. P.; McEwen, A. B.; Yu, C. L.; Eiteneer, B.; Frenklach, M.; Vaghjiani, G. L.; Ravishankara, A. R. Tully, F. P. *J. Phys. Chem.* **1998**, *102*, 8598

(51) (a) Milligan, D. E.; Jacox, M. E. *J. Chem. Phys.* **1971**, *54*, 927. (b) Jacox, M. E. *J. Chem. Phys.* **1988**, *88*, 4598.

(52) (a) Ruscic, B.; Schwarz, M.; Berkowitz, J. *J. Chem. Phys.* **1989**, *91*, 6780. (b) Ruscic, B. and Litorja, M. *Chem. Phys. Lett.* **2000**, *316*, 1, 45.

(53) (a) Radford, H. E.; Wei, W.; Sears, T. J. *J. Phys. Chem.* **1992**, *97*, 3989. (b) Sears, T. J.; Fawzy, W. M.; Johnson, P. M. *J. Phys. Chem.* **1992**, *97*, 3996.

(54) Petty, J. T.; Moore, C. B. *J. Chem. Phys.* **1993**, *99*, 47.

(55) Miyoshi, A.; Matsui, H.; Washida, N. *J. Chem. Phys.* **1994**, *100*, 3532.

(56) Buelow, S.; Radhakrishinan, G.; Catanzarite, J.; Wittig, C. *J. Chem. Phys.* **1985**, *83*, 444.

(57) Radhakrishinan, G.; Buelow, S.; Wittig, C. *J. Chem. Phys.* **1986**, *84*, 727.

(58) Ionov, S. I.; Brucker, G. A.; Jacques, C.; Valachovic, L.; Wittig, C. *J. Chem. Phys.* **1992**, *97*, 9486. Ionov, S. I.; Brucker, G. A.; Jacques, C.; Valachovic, L.; Wittig, C. *J. Chem. Phys.* **1993**, *99*, 6553.

(59) Scherer, N. F.; Khundkar, L. R.; Bernstein, R. B.; Zewail, A. H. *J. Chem. Phys.* **1987**, *87*, 1451.

(60) Scherer, N. F.; Sipes, C.; Bernstein, R. B.; Zewail, A. H. *J. Chem. Phys.* **1990**, *92*, 5239.

(61) Brouard. M.; Hughes, D. W.; Kalogerakis, K. S.; Simons, J. P. *J. Chem. Phys.* **2000**, *12*, 4557.

(62) Rice, J. K.; Baronavski, A. P. *J. Chem. Phys.* **1991**, *94*, 1006.

(63) (a) Kudla, K.; Schatz, G. C.; Wagner, A. F. *J. Chem. Phys.* **1991**, *95*, 1635. (b) Kudla, K.; Koures, A. G.; Harding, L. B.; Schatz, G. C. *J. Chem. Phys.* **1992**, *96*, 7465. (c) Schatz, G. C. *J. Phys. Chem.* **1995**, *99*, 516. (d) Goldfield, E. M.; Gray, S. K.; Schatz, G. C. *J. Chem. Phys.* **1995**, *102*, 8807.

(64) (a) Schatz, G. C.; Fitzcharles, M. S.; Harding, L. B. *Faraday Discuss. Chem. Soc.* **1987**, *84*, 359. (b) Kudla, K.; Schatz, G. C.; Wagner, A. F. *J. Chem. Phys.* **1991**, *95*, 1635. (c) Kudla, K.; Koures, A. G.; Harding, L. B.; Schatz, G. C. *J. Chem. Phys.* **1992**, *96*, 7465.

(65) (a) Clary, D. C.; Schatz, G. C. *J. Chem. Phys.* **1993**, *99*, 4578. (b) Hernandez, M. I.; Clary, D. C. *J. Chem. Phys.* **1994**, *101*, 2779.
(66) Zhang, D. H.; Zhang, J. Z. H. *J. Chem. Phys.* **1995**, *103*, 6512.
(67) Tore, J. Twenty-Seventh Sym. (Int.) on Combustion, The Combustion Institute, Pittsburgh, 1998, 167.
(68) Peyerimhoff, S. D.; Skell, P. S.; May, D. D.; Buenker, R. J. *J. Am. Chem. Soc.* **1982**, *104*, 4515.
(69) Feller, D.; Huyser, E. S.; Borden, W. T.; Davidson, E. R. *J. Am. Chem. Soc.* **1983**, *105*, 1459.
(70) McLean, A. D.; Lengsfield, B. H., III.; Pacansky, J.; Ellinger, Y. *J. Chem. Phys.* **1985**, *83*, 3567.
(71) McLean, A.; D. Ellinger, Y. *Chem. Phys.* **1985**, *94*, 25.
(72) Carmichael, I. *J. Phys. Chem.* **1994**, *98*, 5896.
(73) Aoyagi, M.; Kato, S. *J. Chem. Phys.* **1988**, *88*, 6409.
(74) Diau, E. W. G.; Lin, M. C. *J. Phys. Chem.* **1995**, *99*, 6589.
(75) Klippenstein, S. J.; Wagner, A. F.; Dunbar, R. C.; Wardlaw, D. M. and Robertson, S. H., VARIFLEX: VERSION 1.00, 1999.
(76) Frisch, M. J.; Trucks, G. W.; Head-Gordon, M.; Gill, P. M. W.; Wong, M. W.; Foresman, J. B.; Johnson, B. G.; Schlegel, H. B.; Robb, M. A.; Replogle, E. S.; Gomperts, T.; Andres, J. L.; Raghavachari, K.; Binkley, J. S.; Gonzales, C.; Martin, R. L.; Fox, D. J.; DeFrees, D. J.; Baker, J.; Stewart, J. J. P.; Pople, J. A. Gaussian 92/DFT, Revision B, Gaussian, Inc., Pittsburgh, PA, 1998.
(77) (a) Curtiss, L. A.; Jones, C.; Trucks, G. W.; Raghavachari, K.; Pople, J. A. *J. Chem. Phys.* **1990**, *93*, 2537. (b) Curtiss, L. A.; Raghavachari, K.; Trucks, G. W.; Pople, J. A. *J. Chem. Phys.* **1991**, *94*, 7221.
(78) Mebel, A. M.; Morokuma, K.; Lin, M. C. *J. Chem. Phys.* **1995**, *103*, 7414.
(79) Becke, A. D. *J. Chem. Phys.* **1993**, *98*, 5648.
(80) Becke, A. D. *J. Chem. Phys.* **1992**, *96*, 2155.
(81) Becke, A. D. *J. Chem. Phys.* **1992**, *97*, 9173.
(82) Lee, C.; Yang, W.; Parr, R. G. *Phys. Rev.* **1988**, *B37*, 785.
(83) Head-Gordon, M.; Pople, J. A.; Frisch, M. J. *Chem. Phys. Lett.* **1988**, *153*, 503.
(84) Durant, J. L., Jr.; Rohlfing, C. M. *J. Chem. Phys.* **1993**, *98*, 8031.
(85) Werner, H.-J.; Knowles, P. J. MOLPRO-96 (University of Sussex, Falmer, Brighton, UK 1996).
(86) Gilbert, R. G.; Smith, S. C. *Theory of Unimolecular and Recombination Reactions*; Blackwell Scientific: Carlton, Australia, 1990.
(87) Miller, J. A.; Klippenstein, S. J. *Int. J. Chem. Kinet.* **1999**, *31*, 753.
(88) Miller, J. A.; Klippenstein, S. J.; Robertson, S. H. *J. Phys. Chem. A* **2000**, *104*, 7525.
(89) Miller, J. A.; Klippenstein, S. J. *J. Phys. Chem. A* **2000**, *104*, 2061.
(90) Xia, W. S.; Lin, M. C. *J. Chem. Phys.* **2001**, *114*, 4522.
(91) Holbrook, K. A.; Pilling, M. J.; Robertson, S. H. Unimolecular Reactions, Wiley: 1996.
(92) Troe, J. *J. Chem. Phys.* **1977**, *66*, 6745.
(93) Zhu, R. S.; Lin, M. C. *J. Phys. Chem. A* **2000**, *104* (46), 10807; Xia, W. S., Lin, M. C. *Phys. Chem. Commun. (Electronic Journal)* 13 (2000).
(94) (a) Lester, M. I.; Pond, B. V.; Anderson, D. T.; Harding, L. B.; Wagner, A. F. *J. Chem. Phys.* **2000**, *113*, 9889. (b) Lester, M. I.; Pond, B. V.; Marshall, M. D.; Anderson, D. T.; Harding, L. B.; Wagner, A. F. *Faraday Discuss.* **2001**, *118*, 373.
(95) Chakraborty, D.; Lin, M. C., unpublished work, 1999.
(96) Gonzalez, C.; Schlegel, H. B. *J. Phys. Chem.* **1989**, *90*, 2154.
(97) Jacox, M. E. *J. of Phys. Chem. Ref. Data*, Monograph No. 3−*Vibrational and Electronic Energy Levels of Polyatomic Transient Molecules*, 1994.
(98) Duncan, T. V.; Miller, C. E. *J. Chem. Phys.* **2000**, *113*, 5138.
(99) Chase, M. W. *J. Phys. Chem. Ref. Data Monogr.* **1998**, 9.
(100) Atkinson, R.; Baulch, D. L.; Cox, R. A.; Hampson, R. F.; Kerr, J. A.; Troe, J. *J. Phys. Chem. Ref. Data* **1992**, *21*, 1125.
(101) Hirschfelder, J. O.; Wigner, J. *Chem. Phys.* **1939**, *7*, 616.
(102) Miller, W. H. *J. Chem. Phys.* **1976**, *65*, 2216.
(103) Hirschfelder, J. O.; Curtiss, C. F.; Bird, R. B. Molecular theory of gases and liquids. 2nd ed. John Wiley and Sons Inc., New York, 1964.
(104) Hippler, H.; Troe, J.; Wendelken, H. J. *J. Chem. Phys.* **1983**, *78*, 6709.
(105) Westenberg, A. A.; Wilson, W. E. *J. Chem. Phys.* **1966**, *45*, 338.